

Toward energy-stable multi-phase flow schemes

By J. Nordström[†], H. Collis, R. Brown, M. P. Nchupang[¶] AND S. Mirjalili

On the basis of previous work in Nordström & Malan (2024), we develop a new energy-stable scheme for incompressible multi-phase flows. In particular, we extend our previous work to introduce a multi-phase flow formulation with general interface regularization that complies with the previously developed stable baseline formulation and does not compromise energy stability. This extension can be used for all phase field (diffuse interface) models for which the phase advection equation is in conservative form.

1. Introduction

The basis for nonlinear energy stability of the initial boundary value problem (IBVP) for incompressible multi-phase liquid-gas flows in the volume-of-fluid (VOF) formulation (Hirt & Nichols 1981) was provided in Nordström & Malan (2024). The focus was on the fundamental mathematical groundwork for the IBVP, and specific modeling techniques for interface regularization, such as phase field (diffuse interface) models (Anderson *et al.* 1998; Mirjalili *et al.* 2017; Saurel & Pantano 2018), were not considered.

Related work can be found in, for example, Liu & Walkington (2007); Shen & Yang (2015); Zhiguo & Suchuan (2019), and Mingyang *et al.* (2023), where the original equations are similar, the dependent variables and bounds differ and, most importantly, the boundary conditions are essentially ignored. In Nordström & Malan (2024), the VOF equations were reformulated into a set of skew-symmetric equations that were straightforward to discretize using summation-by-parts (SBP) operators. Augmented with new boundary conditions, this new formulation led to provable energy stability for the semi-discrete approximation.

The remainder of this report is structured as follows. In Section 2, the previous formulation is outlined. Section 3 sketches the SBP discretization in space and comments on the time advancement. Section 4 is devoted to a new general interface regularization formulation that complies with the previously developed stable baseline formulation. Section 5 presents preliminary numerical results. Conclusions and an outlook are given in Section 6.

2. Previous work

All details and material in this section can be found in Nordström & Malan (2024).

[†] Department of Mathematics, Linköping University, Sweden and Department of Mathematics and Applied Mathematics, University of Johannesburg, South Africa

[¶] Department of Applied Mathematics, Stellenbosch University, South Africa

2.1. The skew-symmetric reformulation

The classical one-fluid VOF formulation for an incompressible viscous liquid (l) and gas (g) mixture in two dimensions (2D) using Einstein's summation convention reads

$$\begin{aligned}\partial_t \alpha + u_j \partial_j \alpha &= 0 \\ \partial_t u_i + u_j \partial_j u_i &= \partial_j \tau_{ij} / \rho, \quad i = 1, 2 \\ \partial_j u_j &= 0.\end{aligned}\tag{2.1}$$

The derivatives involved are denoted $\partial_t \psi = \psi_{,t} = \partial \psi / \partial t$ and $\partial_j \psi = \psi_{,j} = \partial \psi / \partial x_j$, where α is the volume fraction of the liquid, u_j is velocity in direction x_j , $\tau_{ij} = \tau_{ij}^* - \delta_{ij} p$ is the stress tensor, $\tau_{ij}^* = [\mu(u_{i,j} + u_{j,i})]$ is the viscous stress tensor and p is pressure. Furthermore, $\rho = \alpha \rho_l + (1 - \alpha) \rho_g$ and $\mu = \alpha \mu_l + (1 - \alpha) \mu_g$ are the volume-averaged density and viscosity, respectively. The external gravity forces with no impact on stability were neglected.

The formulation of Eq. (2.1) was modified using the density instead of the volume fraction, the new variables $\Phi = [\phi_0, \phi_1, \phi_2, \phi_3]^T = [\sqrt{\rho}, \sqrt{\rho} u_1, \sqrt{\rho} u_2, p]$ and the notation $S_{1j} = \tau_{1j}$, $S_{2j} = \tau_{2j}$ and $S_{3j} = -u_j$ to yield

$$\tilde{I} \partial_t \Phi + \frac{1}{2} [\partial_j (\tilde{A}_j \Phi) + \tilde{A}_j \partial_j \Phi] = \tilde{B} \partial_j S_j.\tag{2.2}$$

In Eq. (2.2), $\tilde{I} = \text{diag}[1, 1, 1, 0]$, $\tilde{A}_j = \text{diag}[u_j, u_j, u_j, 0]$, $\tilde{B} = \text{diag}[0, 1/\phi_0, 1/\phi_0, 1]$, $S_j = (0, S_{1j}, S_{2j}, S_{3j})^T$ were introduced and the fact that $A_{j,j}$ vanishes was used.

2.2. Nonlinear boundary conditions

The energy method (see Nordström & Malan (2024)) lead to the following energy rate

$$\frac{d}{dt} \|\Phi\|_I^2 + 2 \int_{\Omega} u_{i,j} \tau_{ij}^* d\Omega + \oint_{\partial\Omega} BT ds = 0,\tag{2.3}$$

where the second term $[u_{i,j} \tau_{ij}^* = 2u_{i,i}^2 + (u_{1,2} + u_{2,1})^2 \geq 0]$ provides dissipation and the third boundary term is given by

$$BT = \Phi_1^T A \Phi_1 - 2[u_n(\tau_n - p) + u_t \tau_t].\tag{2.4}$$

In Eq. (2.4), $A = \text{diag}[u_n, u_n, u_n]$ and $\Phi_1^T = [\phi_0, \phi_n, \phi_t] = [\phi_0, \phi_0 u_n, \phi_0 u_t]$. The subscripts n and t denote components normal and tangential to $\partial\Omega$. For the stress term in Eq. (2.4) we use $\tau^T = [\tau_1, \tau_2] = [\tau_{1j}^* n_j, \tau_{2j}^* n_j]$ and the rotation matrix N [given in Eq. (2.15) below] to obtain $\mathbf{u}^T \tau = \mathbf{u}^T (N^T N) \tau = (N \mathbf{u})^T (N \tau) = [u_n, u_t] \cdot [\tau_n, \tau_t]^T$.

The boundary term in Eq. (2.4) can be written in vector-matrix-vector form as

$$BT = \begin{pmatrix} \Phi_1 \\ \Phi_2 \end{pmatrix}^T \begin{pmatrix} A & B \\ B^T & 0 \end{pmatrix} \begin{pmatrix} \Phi_1 \\ \Phi_2 \end{pmatrix}, \quad \Phi_2 = \begin{pmatrix} p \\ \tau_n \\ \tau_t \end{pmatrix}, \quad B = \frac{1}{\phi_0} \begin{pmatrix} 0 & 0 & 0 \\ 1 & -1 & 0 \\ 0 & 0 & -1 \end{pmatrix}\tag{2.5}$$

while Φ_1 and A are given above. By rotating the boundary term to diagonal form, we get

$$BT = \begin{pmatrix} W_1 \\ W_2 \end{pmatrix}^T \begin{pmatrix} \Lambda_1 & 0 \\ 0 & \Lambda_2 \end{pmatrix} \begin{pmatrix} W_1 \\ W_2 \end{pmatrix} \quad \text{where} \quad \Lambda_1 = \frac{1}{u_n} I, \Lambda_2 = -\Lambda_1.\tag{2.6}$$

The details in Eq. (2.6) seen in Eq. (2.7) reveal that five independent variables are

involved in the boundary conditions.

$$W_1 = A\Phi_1 + B\Phi_2 = \frac{1}{\phi_0} \begin{pmatrix} \phi_n\phi_0 \\ \phi_n^2 - (\tau_n - \phi_3) \\ \phi_n\phi_t - \tau_t \end{pmatrix}, W_2 = B\Phi_2 = \frac{1}{\phi_0} \begin{pmatrix} 0 \\ -(\tau_n - \phi_3) \\ -\tau_t \end{pmatrix}. \quad (2.7)$$

2.2.1. Boundary conditions of inflow-outflow type with nonzero external data

We start by determining the number of boundary conditions (Nordström & Hagstrom 2020) required at inflow-outflow boundaries.

- At inflow $u_n < 0$, $W_1^T \Lambda_1 W_1 < 0$ and we need three conditions since W_1 has three components.

- At outflow $u_n > 0$, $W_2^T \Lambda_2 W_2 < 0$ and we need two conditions since W_2 has two nonzero components.

Following Nordström (2017) (and ignoring the dissipation), the boundary conditions are applied weakly by inserting Eq. (2.6) and a lifting operator into Eq. (2.3),

$$\frac{d}{dt} \|\Phi\|_I^2 + \oint_{\partial\Omega} \begin{pmatrix} W_1 \\ W_2 \end{pmatrix}^T \begin{pmatrix} \Lambda_1 & 0 \\ 0 & \Lambda_2 \end{pmatrix} \begin{pmatrix} W_1 \\ W_2 \end{pmatrix} ds + 2 \int_{\Omega} \Phi^T L(\Sigma BC) d\Omega \leq 0. \quad (2.8)$$

Here BC denotes the boundary conditions, Σ is a penalty matrix and L is a lifting operator implementing boundary conditions weakly. It is defined by $\int_{\Omega} \psi^T L(\phi) d\Omega = \oint_{\partial\Omega} \psi^T \phi ds$, where ψ and ϕ are smooth vector fields.

Following Nordström (2024), we use the weak characteristic-like boundary condition

$$BC = \sqrt{|\Lambda^-|} W^- - \mathbf{G} = 0, \quad (2.9)$$

where Λ^- and W^- are functions of the solution and \mathbf{G} is external data. To implement inflow boundary conditions weakly, we need an operator T_1 so that

$$W^- = W_1 = A\Phi_1 + B\Phi_2 = \frac{1}{\phi_0} \begin{pmatrix} \phi_n\phi_0 \\ \phi_n^2 - (\tau_n - \phi_3) \\ \phi_n\phi_t - \tau_t \end{pmatrix} = T_1\Phi = (\Phi^T T_1^T)^T. \quad (2.10)$$

At an outflow boundary, we require an operator T_2 so that

$$W^- = W_2 = B\Phi_2 = \frac{1}{\phi_0} \begin{pmatrix} 0 \\ -(\tau_n - \phi_3) \\ -\tau_t \end{pmatrix} = T_2\Phi = (\Phi^T T_2^T)^T. \quad (2.11)$$

Implementing the boundary condition of Eq. (2.9) weakly into Eq. (2.8) and using $\Sigma = T^T \sigma_0 \sqrt{|\Lambda^-|}$, ($T = T_1$ or T_2) and $\sigma_0 = 1$ yield the following final estimate of all surface terms

$$BT = W^{+T} \Lambda^+ W^- + \left(W^- \sqrt{|\Lambda^-|} - \mathbf{G} \right)^T \left(W^- \sqrt{|\Lambda^-|} - \mathbf{G} \right) - \mathbf{G}^T \mathbf{G} \geq -\mathbf{G}^T \mathbf{G}. \quad (2.12)$$

2.2.2. Boundary conditions of solid wall type with zero external data

At solid wall boundaries where $u_n = 0$, we work directly on BT in Eq. (2.4) which gives

$$BT = [\Phi_1^T A\Phi_1 + 2\Phi_1^T \Sigma_1 BC_1] + [2\Phi_1^T B\Phi_2 + 2\Phi_1^T \Sigma_2 BC_2]. \quad (2.13)$$

Only the two boundary conditions $u_n = u_t = 0$ are available at a solid wall. For reasons of accuracy, they must cancel both bracketed terms in Eq. (2.13).

For the first term in brackets in Eq. (2.13), we set $\Sigma_1 = R_1^T \Sigma'_1$ with $R_1 \Phi = \Phi_1$ to obtain

$$\Phi_1^T A \Phi_1 + 2\Phi_1^T \Sigma_1 B C_1 = \Phi_1^T A \Phi_1 + 2\Phi_1^T \Sigma'_1 B C_1, \quad (2.14)$$

where

$$R_1 = \begin{pmatrix} 1 & 0 & 0 & 0 \\ 0 & n_1 & n_2 & 0 \\ 0 & -n_2 & n_1 & 0 \end{pmatrix} \quad \text{and} \quad \begin{pmatrix} n_1 & n_2 \\ -n_2 & n_1 \end{pmatrix} = N. \quad (2.15)$$

Next we insert $\Sigma'_1 = \sigma_1 = -1/2$ and $BC_1 = A\Phi_1$ into Eq. (2.14) to give

$$\Phi_1^T A \Phi_1 + 2\Phi_1^T \Sigma'_1 B C_1 = \Phi_1^T A \Phi_1 + 2\Phi_1^T (\sigma_1 A \Phi_1) = \Phi_1^T A \Phi_1 [1 + 2\sigma_1] = 0. \quad (2.16)$$

Accuracy is proven by noting that u_n is forced to zero by $\Sigma_1 B C_1$, since

$$\Sigma_1 B C_1 = \sigma_1 R_1^T A \Phi_1 = \sigma_1 R_1^T \Phi_1 u_n.$$

For the second term in brackets in Eq. (2.13), we set $\Sigma_2 = R_2^T \Sigma'_2$ with $R_2 \Phi = \Phi_2$ to obtain

$$2\Phi_1^T B \Phi_2 + 2\Phi_1^T \Sigma_2 B C_2 = 2(B\Phi_2)^T \Phi_1 + 2\Phi_1^T \Sigma'_2 B C_2, \quad (2.17)$$

where $R_2 = P_e T_r S_c$, $S_c = \text{diag}[1, 1/\phi_0, 1/\phi_0, 1]$ and

$$P_e = \begin{pmatrix} 0 & 0 & 1 \\ 1 & 0 & 0 \\ 0 & 1 & 0 \end{pmatrix}, \quad T_r = \begin{pmatrix} 0 & T_{r11} & T_{r11} & 0 \\ 0 & T_{r21} & T_{r22} & 0 \\ 0 & 0 & 0 & 1 \end{pmatrix}, \quad T_r = \mu N \left[\begin{pmatrix} 2n_1 & n_2 \\ 0 & n_1 \end{pmatrix} x + \begin{pmatrix} n_2 & 0 \\ n_1 & 2n_2 \end{pmatrix} y \right].$$

Setting $\Sigma'_2 = \sigma_2 = -1$ and $BC_2 = B^T \Phi_1$ into Eq. (2.17),

$$2(B\Phi_2)^T \Phi_1 + 2\Phi_1^T \Sigma'_2 B C_2 = 2(B\Phi_2)^T \Phi_1 + 2\sigma_2 (B\Phi_2)^T \Phi_1 = 2(1 + \sigma_2) (B\Phi_2)^T \Phi_1 = 0.$$

Accuracy is proven by noting that Σ_{22} forces u_n and u_t to zero since,

$$\Sigma_{22} = R_2^T \Sigma'_{22} = \sigma_2 R_2^T B^T \Phi_1 = \sigma_2 R_2^T B^T \begin{pmatrix} \phi_0 \\ \phi_n \\ \phi_t \end{pmatrix} = \sigma_2 R_2^T \begin{pmatrix} u_n \\ -u_n \\ -u_t \end{pmatrix}.$$

3. A straightforward nonlinear numerical approximation

The focus in this report is on the continuous analysis, but for clarity we now show how the continuous formulation can be mimicked discretely. We also illustrate the time-advancement procedure.

3.1. The spatial discretization

The semi-discrete version of Eq. (2.2) (ignoring boundary conditions) using SBP operators $\mathbf{D}_{\mathbf{x}_j}$ (Svärd & Nordström 2014; Fernández *et al.* 2014) can be written

$$\tilde{\mathbf{I}} \frac{d\vec{\Phi}}{dt} + \frac{1}{2} \left[\mathbf{D}_{\mathbf{x}_j} (\mathbf{A}_j \vec{\Phi}) + \mathbf{A}_j \mathbf{D}_{\mathbf{x}_j} \vec{\Phi} \right] = \mathbf{B} \mathbf{D}_{\mathbf{x}_j} \mathbf{S}_j, \quad (3.1)$$

where $\tilde{\mathbf{I}} = \tilde{I} \otimes I$, $I = I_x \otimes I_y$ and $\vec{\Phi} = (\vec{\phi}_0^T, \vec{\phi}_1^T, \vec{\phi}_2^T, \vec{\phi}_3^T)^T$ include approximations of $\Phi = (\phi_0, \phi_1, \phi_2, \phi_3)^T$ in each of the $N \times M$ nodes. The matrix elements of \mathbf{A}_j, \mathbf{B} are matrices with node values of the matrix elements in \tilde{A}_j, \tilde{B} given in Section 2 injected on

the diagonal as exemplified for the $n \times n$ matrix C below

$$C = \begin{pmatrix} c_{11} & \cdots & c_{1n} \\ \vdots & \ddots & \vdots \\ c_{n1} & \cdots & c_{nn} \end{pmatrix}, \quad \mathbf{C} = \begin{pmatrix} \mathbf{c}_{11} & \cdots & \mathbf{c}_{1n} \\ \vdots & \ddots & \vdots \\ \mathbf{c}_{n1} & \cdots & \mathbf{c}_{nn} \end{pmatrix}, \quad \mathbf{c}_{ij} = \text{diag}(c_{ij}(x_1, y_1), \dots, c_{ij}(x_N, y_M)). \quad (3.2)$$

Moreover, $\mathbf{D}_{\mathbf{x}_j} = I_4 \otimes D_{x_j}$, $D_{x_1} = D_x \otimes I_y$ and $D_{x_2} = I_x \otimes D_y$, where $D_{x,y} = P_{x,y}^{-1} Q_{x,y}$ are 1D SBP difference operators, $P_{x,y}$ are positive definite diagonal quadrature matrices, $Q_{x,y}$ satisfies the SBP constraint $Q_{x,y} + Q_{x,y}^T = B_{x,y} = \text{diag}[-1, 0, \dots, 0, 1]$, \otimes denotes the Kronecker product and I with subscripts denotes identity matrices. All matrices have appropriate sizes so that the matrix-matrix and matrix-vector operations are defined. Based on the 1D SBP operators, the 2D SBP relations mimicking integration-by-parts are

$$\vec{U}^T \mathbf{P} \mathbf{D}_{\mathbf{x}_j} \vec{V} = -(\mathbf{D}_{\mathbf{x}_j} \vec{U})^T \mathbf{P} \vec{V} + \vec{U}^T \mathbf{B}_{\mathbf{x}_j} \vec{V}, \quad \vec{u}^T P D_{x_j} \vec{v} = -(D_{x_j} \vec{u})^T P \vec{v} + \vec{u}^T B_{x_j} \vec{v}, \quad (3.3)$$

where $\vec{U}^T \mathbf{B}_{\mathbf{x}_j} \vec{V}$ and $\vec{u}^T B_{x_j} \vec{v}$ contain numerical integration along rectangular domain boundaries. In Eq. (3.3) we have also used $\mathbf{P} = I_4 \otimes P$, $P = P_x \otimes P_y$, $\mathbf{B}_{\mathbf{x}_j} = I_4 \otimes B_{x_j}$, $B_{x_1} = B_x \otimes P_y$ and $B_{x_2} = P_x \otimes B_y$.

The discrete energy method [multiply Eq. (3.1) from the left with $2\vec{\Phi}^T \mathbf{P}$] yields

$$2\vec{\Phi}^T \mathbf{P} \tilde{\mathbf{I}} \frac{d\vec{\Phi}}{dt} + \vec{\Phi}^T (\mathbf{P} \mathbf{D}_{\mathbf{x}_j} \mathbf{A}_j + \mathbf{A}_j \mathbf{P} \mathbf{D}_{\mathbf{x}_j}) \vec{\Phi} = 2\vec{\Phi}^T \mathbf{B} \mathbf{P} \mathbf{D}_{\mathbf{x}_j} \mathbf{S}_j, \quad (3.4)$$

since \mathbf{A}_j and \mathbf{B} commute with \mathbf{P} . Using the notation $\|\vec{\Phi}\|_{\mathbf{P}}^2 = \vec{\Phi}^T \tilde{\mathbf{P}} \vec{\Phi} = \vec{\Phi}^T \mathbf{P} \tilde{\mathbf{I}} \vec{\Phi}$ and the symmetric part of $\mathbf{P} \mathbf{D}_{\mathbf{x}_j} \mathbf{A}_j + \mathbf{A}_j \mathbf{P} \mathbf{D}_{\mathbf{x}_j}$ and after applying the SBP relations Eq. (3.3), we obtain the final semi-discrete energy rate

$$\frac{d}{dt} \|\vec{\Phi}\|_{\mathbf{P}}^2 + 2(D_{x_j} \vec{u}_i)^T P \tau_{ij}^* + \vec{\Phi}^T (\mathbf{B}_{\mathbf{x}_j} \mathbf{A}_j) \vec{\Phi} - 2\vec{u}_i^T B_{x_j} \tau_{ij} = 0. \quad (3.5)$$

The semi-discrete energy rate of Eq. (3.5) mimics the continuous energy rate of Eq. (2.3) perfectly on a rectangular domain. The second term from the left in Eq. (3.5) is the dissipation numerically integrated over the domain and the two terms that follow contain the boundary terms numerically integrated along the boundary.

3.2. The time discretization

The resulting energy-stable scheme in Eq. (3.1) (augmented with weak penalty terms) is discretized in time as it stands; no pressure Poisson equation is used. We discretize the temporal derivative in Eq. (3.1) implicitly, leading to a fully discrete formulation. We presently consider the second-order backward differentiation formula (BDF2) method. The fully discrete approximation of Eq. (2.2) becomes

$$H(\vec{\Phi}^{n+2}) = \tilde{\mathbf{I}} \frac{3\vec{\Phi}^{n+2} - 4\vec{\Phi}^{n+1} + \vec{\Phi}^n}{2\Delta t} + D(\vec{\Phi}^{n+2}) \vec{\Phi}^{n+2} = \mathbf{0}, \quad (3.6)$$

where superscripts $n+2$, $n+1$ and n denote the solution at three consecutive time levels and Δt is the time step. Further, $D(\cdot)$ denotes the nonlinear discrete spatial operator, including weak boundary conditions. Equation (3.6) is a system of nonlinear equations that can be solved using numerical routines such as Newton's method. Here, we follow the procedure described in Nordström *et al.* (2024) and linearize Eq. (3.6) with Newton's

method

$$\vec{\Phi}^{n+2} = \vec{\Phi}^{n+1} - \mathbf{J}^{-1} H(\vec{\Phi}^{n+1}, \vec{\Phi}^n), \quad (3.7)$$

where the intermediate solutions Φ^{n+1} and Φ^n in Eqs. (3.6) – (3.7) are computed in previous iterations. In Eq. (3.7), \mathbf{J}^{-1} is the inverse matrix of the exact Jacobian matrix of H . For more details see Nordström *et al.* (2024). Equation (3.7) is then solved iteratively until

$$\|\vec{\Phi}^{n+2} - \vec{\Phi}^{n+1}\|_{\mathbf{p}}^2 \leq tol \quad (3.8)$$

is reached, where tol is the specified tolerance.

4. An interface-regularized formulation

The one-fluid sharp-interface formulation described in Section 2 is often modified at the partial differential equation (PDE) level to regularize the interfaces between phases (Anderson *et al.* 1998; Mirjalili *et al.* 2017; Saurel & Pantano 2018). The interface regularization (using phase field methods) aims for fixed interface thicknesses that can be resolved on a reasonably coarse grid with standard numerical schemes. In recent years, phase field methods have emerged as a popular alternative for modeling two-phase flows. In particular, conservative phase field methods, using the second-order conservative Allen-Cahn (also known as conservative diffuse interface) equation or the fourth-order Cahn-Hilliard equation, have received the most attention because they achieve interface regularization while retaining conservation of mass of each phase. In particular, the governing equations for these conservative phase field models can be written as (Khanwale *et al.* 2020; Mirjalili *et al.* 2020; Mirjalili & Mani 2021)

$$\begin{aligned} \partial_t \alpha + \partial_j (u_j \alpha) &= \partial_j r_j \\ \partial_t (\rho u_i) + \partial_j (\rho u_j u_i) &= \partial_j \tau_{ij} + \partial_j (R_j u_i), \quad i = 1, 2 \\ \partial_j u_j &= 0, \end{aligned} \quad (4.1)$$

where r_j is the regularization flux, defined using the phase field variable α (liquid volume fraction) and its derivatives, and $R_j = (\rho_l - \rho_g)r_j$ is the mass flux.

In order to convert the above system of equations to skew-symmetric form, we take inspiration from Nordström & Malan (2024) and rewrite the equations using the same variables $\Phi^T = (\sqrt{\rho}u_0, \sqrt{\rho}u_1, \sqrt{\rho}u_2, P/(\sqrt{\rho_0}u_0))$, where for dimensional consistency, we have included u_0 and ρ_0 as constants equal to 1, with units of m/s, and kg/m³, respectively. With some algebra, it can be shown that the system of equations given in Eq. 4.1 can be written in skew-symmetric form as

$$\tilde{I} \partial_t \Phi + \frac{1}{2} [\partial_j (\tilde{A}_j \Phi) + \tilde{A}_j \partial_j \Phi] = \tilde{B} \partial_j S_j, \quad (4.2)$$

where \tilde{I} and \tilde{A}_j remain unchanged as in Eq. (2.2).

As such, apart from unity constants for dimensional consistency, the left-hand-side (LHS) of Eq. (4.2) remains unchanged with respect to the original VOF formulation. The right-hand-side (RHS) matrices are modified because of the regularization fluxes

into

$$\tilde{B} = \begin{bmatrix} 1/\sqrt{\rho} & 0 & 0 & 0 \\ -u_1/(u_0\sqrt{\rho}) & 1/\sqrt{\rho} & 0 & 0 \\ -u_2/(u_0\sqrt{\rho}) & 0 & 1/\sqrt{\rho} & 0 \\ 0 & 0 & 0 & 1/\sqrt{\rho_0} \end{bmatrix} \quad (4.3)$$

and

$$S_j = \begin{bmatrix} u_0 R_j / 2 \\ \tau_{1j} + u_1 R_j \\ \tau_{2j} + u_2 R_j \\ -\rho_0 u_0 u_j \end{bmatrix}. \quad (4.4)$$

Recall that R is the flux of the interface regularization term in the mass equation, with units of $\text{kg}/(\text{m}^2\text{s})$. The skew-symmetric formulation derived above holds for any choice of this regularization flux.

As a specific example, Mirjalili *et al.* (2020) and Mirjalili & Mani (2021) introduced the second-order conservative phase field model for which R_j is given by

$$R_j = \gamma \left[\epsilon \frac{\partial \rho}{\partial x_j} - \frac{(\rho_l - \rho)(\rho - \rho_g)}{\rho_l - \rho_g} n_j^r \right], \quad (4.5)$$

where \vec{n}^r is the normal vector for the interface, defined as

$$n_j^r = \frac{\partial \rho / \partial x_j}{((\partial \rho / \partial x_k)(\partial \rho / \partial x_k))^{1/2}}, \quad (4.6)$$

and γ and ϵ are the two parameters of the model, with units of m/s and m , representing the strength of the regularization and the interface thickness, respectively.

4.1. Energy equation for the interface-regularized formulation

Again, we follow Nordström & Malan (2024) to derive the energy equation for the interface-regularized formulation. Multiplying Φ^T into Eq. (4.2), we obtain

$$\frac{d}{dt} \|\Phi\|_I^2 + \oint_{\partial\Omega} \Phi^T (n_j \tilde{A}_j) \Phi ds = 2 \int_{\Omega} \Phi^T \tilde{B} \partial_j S_j d\Omega, \quad (4.7)$$

where the first term represents the rate of change of energy,

$$\frac{d}{dt} \|\Phi\|_I^2 = \frac{d}{dt} \int_{\Omega} \rho (u_0^2 + u_1^2 + u_2^2) d\Omega, \quad (4.8)$$

and the second term on the LHS is a boundary term. The RHS of Eq. (4.7) is expanded as

$$\begin{aligned} \oint_{\Omega} \Phi^T \tilde{B} \partial_j S_j d\Omega &= \oint_{\partial\Omega} (u_i \tau_{ij} n_j) ds - \int_{\Omega} u_{i,j} \tau_{ij}^* d\Omega + \\ &\int_{\Omega} \left(\frac{u_0^2}{2} R_{j,j} - \frac{u_1^2}{2} R_{j,j} - \frac{u_2^2}{2} R_{j,j} + u_1 (u_1 R_j) j + u_2 (u_2 R_j) j \right) d\Omega = \\ &\oint_{\partial\Omega} (u_i \tau_{ij} n_j) ds - \int_{\Omega} u_{i,j} \tau_{ij}^* d\Omega + \oint_{\partial\Omega} \frac{1}{2} (u_0^2 + u_1^2 + u_2^2) R_j n_j ds. \end{aligned} \quad (4.9)$$

Hence, the energy equation can be rewritten as

$$\frac{d}{dt} \|\Phi\|_I^2 + 2 \int_{\Omega} u_{i,j} \tau_{ij}^* d\Omega + \oint_{\partial\Omega} BT ds = 0, \quad (4.10)$$

where the second term is a volume term that provides viscous dissipation, and the boundary term is

$$BT = \Phi_1^T A \Phi_1 - 2[u_n(\tau_n - p) + u_t \tau_t] + \Phi_1^T R \Phi_1, \quad (4.11)$$

where $A = \text{diag}[u_n, u_n, u_n]$, $\Phi_1^T = [\sqrt{\rho}u_0, \sqrt{\rho}u_n, \sqrt{\rho}u_t]$, and $R = -\text{diag}[R_n, R_n, R_n]/\rho$. Crucially, with the proposed interface-regularized skew-symmetric formulation, the addition of the regularizing terms did not result in any new volumetric terms in the energy equation. Instead, the effect of the regularizing flux appears in a boundary term that is identically zero if the normal regularizing flux into the domain (R_n) is zero. Indeed, this is a common choice in phase field simulations, even in the presence of contact lines (Brown *et al.* 2022). One may also note that the structure of the terms $\Phi_1^T A \Phi_1$ and $\Phi_1^T R \Phi_1$ are the same, which will influence the choice of boundary conditions.

5. Numerical results

The following section verifies the implementation of the energy-stable VOF formulation without interface regularization terms. A simulation of a two-phase droplet evolving in an inviscid vortex is used to show the convergence of the solver to the expected order of accuracy. It also confirms the numerical energy stability of the proposed formulation. The initial condition of the simulation is given by

$$\rho = (\rho_l - \rho_g) \left[0.5 \left(1 + \tanh \left(\frac{R - \sqrt{(x - x_c)^2 + (y - y_c)^2}}{2\epsilon\Delta} \right) \right) \right] + \rho_g \quad (5.1)$$

$$u = \pi \sin(\pi x)^2 \sin(2\pi y) \quad (5.2)$$

$$v = -\pi \sin(2\pi x) \sin(\pi y) \quad (5.3)$$

$$p = \cos(\pi x) \sin(\pi y), \quad (5.4)$$

where $\rho_l = 2$, $\rho_g = 1$, $R = 0.2$, $\epsilon = 1.5$, $(x_c, y_c) = (0.5, 0.6)$, $x = [0, 1]$, and $y = [0, 1]$. Figure 1 shows the evolution of the drop over time using the fourth-order accurate SBP363 spatial operators with a domain resolution of $(N_x, N_y) = (51, 51)$ and BDF2 for time integration with a constant $dt = 0.0125$. Over the duration of the simulation the droplet is deformed and the simulation stays stable and convergent to a residual error tolerance of 1×10^{-11} . At late times small spatial dispersion errors can be seen as a result of the absence of dissipation in spatial SBP operators (central scheme in the interior) being applied to increasingly sharp gradients in density. Extending the code to include the interface regularization terms described in Section 4 is expected to remove these errors.

As shown in Eqs. (2.3)-(2.4) the energy decay for inviscid flow with solid walls is zero, rendering a constant energy as time passes. In the discrete case, this ideal result should be approached as the mesh is refined. With SBP operators in space and weak boundary conditions, no dissipation is introduced by the spatial approximation. To verify the energy stability of the system, the energy in the simulation is quantified as $\|\vec{\Phi}\|_{\mathbf{P}}^2 = \vec{\Phi}^T \mathbf{P} \vec{\Phi}$ and plotted over time while decreasing dt . Figure 2 shows the convergence toward a constant energy solution over time with decreasing dt , verifying that the time discretization is the source of the discrete energy decay. Future work will investigate using nondissipative SBP operators in time (instead of the diffusive BDF-type schemes). The change of time integrator will also guarantee energy stability for the fully discrete approximation.

Lastly, verification of the accuracy of the scheme can be shown by the convergence of the wall-normal velocity u_n toward zero with increasing spatial resolution. The metric is

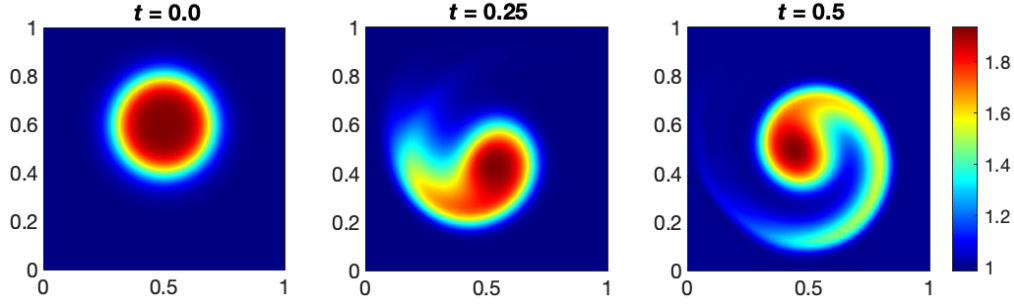


FIGURE 1. Evolution of a droplet in an inviscid vortex over time using the fourth-order SBP363 spatial operators with $(N_x, N_y) = (51, 51)$.

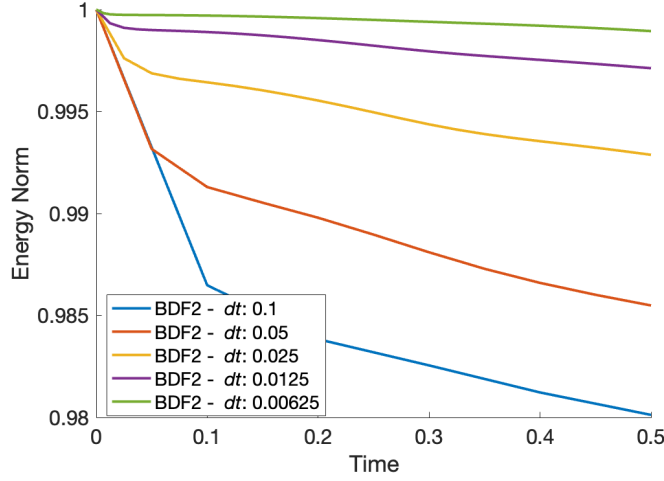


FIGURE 2. Energy stability of a droplet in an inviscid vortex over time using the second-order SBP121 spatial operators with $(N_x, N_y) = (51, 51)$.

the root-mean-square value of u_n over all four wall boundaries, calculated at time $t = 0.1$, and this metric is calculated for four spatial resolutions: $(N_x, N_y) = (16, 16)$, $(32, 32)$, $(64, 64)$, and $(128, 128)$. The expected rate of convergence for the various SBP schemes is half the interior order of accuracy, plus one, and Figure 3 shows that each scheme does in fact converge at the expected rate. Future work will include additional verification using the method of manufactured solutions.

6. Conclusions and future work

On the basis of previous work in Nordström & Malan (2024), we developed a code for the baseline scheme and a new regularization formulation of the interface that can be made energy stable by imposing suitable boundary conditions. We performed preliminary calculations using the baseline scheme and showed correct convergence rates for the case with a spinning inviscid drop in a box. In addition, we showed that energy was preserved for small time steps.

In future work we will introduce the interface regularization and develop a stable

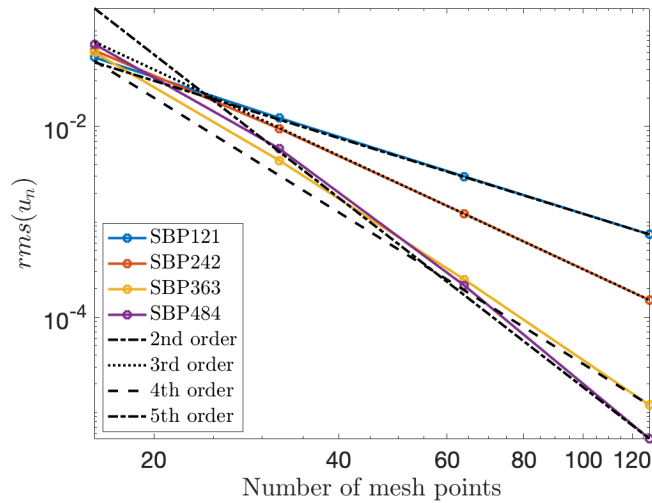


FIGURE 3. Mesh convergence of the root-mean-square value of wall-normal velocity u_n at time $t = 0.1$ for SBP schemes of various orders of accuracy. Each scheme converges at the expected rate, which is half the interior order of accuracy, plus one.

and weak solid wall boundary implementation. Next, we will introduce viscous terms and repeat that action. Finally, we will insert weak inflow-outflow boundary conditions, both inviscid and viscous ones. All implementation steps described above will be verified using the method of manufactured solutions. Subsequently, we will perform extensive testing on well known test cases for multi-phase flow. We will also replace the current time-integration scheme BDF2 with SBP in time which is nondissipative and leads to provably energy-stable fully discrete approximations.

REFERENCES

- ANDERSON, D. M., MCFADDEN, G. B. & WHEELER, A. A. 1998 Diffuse-interface methods in fluid mechanics. *Annu. Rev. Fluid Mech.* **30**, 139–165.
- BROWN, R., MIRJALILI, S., KHANWALE, M., GANAPATHYSUBRAMANIAN, B. & MANI, A. 2022 A generalized Navier boundary condition for modeling contact lines using second-order conservative phase-field methods. *Annual Research Briefs*, Center for Turbulence Research, Stanford University, pp 193–201.
- FERNÁNDEZ, D. C. D. R & HICKEN, J. E. & ZINGG, D. W. 2014 Review of summation-by-parts operators with simultaneous approximation terms for the numerical solution of partial differential equations. *Comput. Fluids* **95**, 171–196.
- HIRT, C. AND NICHOLS, B. 1981 VOF method for the dynamics of free boundaries. *J. Comput. Phys.* **39**, 201–225.
- KHANWALE, M. A., LOFQUIST, A. D., SUNDAR, H., ROSSMANITH, J. A. & GANAPATHYSUBRAMANIAN, B. 2020 Simulating two-phase flows with thermodynamically consistent energy stable Cahn-Hilliard Navier-Stokes equations on parallel adaptive octree based meshes. *J. Comput. Phys.* **419**, 109674.

- LIU, C. & WALKINGTON, N. J. 2007 Convergence of numerical approximations of the incompressible Navier–Stokes equations with variable density and viscosity. *SIAM J. Numer. Anal.* **45**, 1287–1304.
- MINGYANG, P., CHENGXING, F., WENXING, Z., FENGYU J. & DONGDONG, H. 2023 Linear, second-order, unconditionally energy stable scheme for an electrohydrodynamic model with variable density and conductivity. *Commun. Nonlinear Sci.* **125**, 107329.
- MIRJALILI, S., JAIN, S. S. & DODD, M. 2017 Interface-capturing methods for two-phase flows: an overview and recent developments. *Annual Research Briefs*, Center for Turbulence Research, Stanford University, pp 117–135.
- MIRJALILI, S., IVEY, C. B. & MANI, A. 2019 Comparison between the diffuse interface and volume of fluid methods for simulating two-phase flows. *Int. J. Multiphas. Flow* **116**, 221–238.
- MIRJALILI, S., IVEY, C. B. & MANI, A. 2020 A conservative diffuse interface method for two-phase flows with provable boundedness properties. *J. Comput. Phys.* **401**, 109006.
- MIRJALILI, S. & MANI, A. 2021 Consistent, energy-conserving momentum transport for simulations of two-phase flows using the phase field equations. *J. Comput. Phys.* **426**, 109918.
- NORDSTRÖM, J. 2017 A roadmap to well posed and stable problems in computational physics. *J. Sci. Comput.* **71**, 365–385.
- NORDSTRÖM, J. & HAGSTROM T. H. 2020 The number of boundary conditions for initial boundary value problems. *SIAM J. Numer. Anal.* **58**, 2818–2828.
- NORDSTRÖM, J. 2024 Nonlinear boundary conditions for initial boundary value problems with applications in computational fluid dynamics. *J. Comput. Phys.* **498**, 112685.
- NORDSTRÖM, J. & LAURÉN, F. & ÅLUND, O. 2024 An explicit Jacobian for Newton’s method applied to nonlinear initial boundary value problems in summation-by-parts form. *AIMS Math.*, **9**, 23291–23312.
- NORDSTRÖM, J. & MALAN, A. G. 2024 An energy stable nonlinear incompressible multi-phase flow formulation. *arXiv:2406.19525*.
- SAUREL, R. & PANTANO, C. 2018 Diffuse-interface capturing methods for compressible two-phase flows. *Annu. Rev. Fluid Mech.* **50**, 105–130.
- SHEN, J. & YANG, X. 2015 Decoupled, energy stable schemes for phase-field models of two-phase incompressible flows. *SIAM J. Numer. Anal.* **53**, 279–296.
- SVÄRD, M. & NORDSTRÖM, J. 2014 Review of summation-by-parts schemes for initial–boundary-value problems. *J. Comput. Phys.* **268**, 17–38.
- ZHIGUO, Y. & SUCHUAN, D. 2019 An unconditionally energy-stable scheme based on an implicit auxiliary energy variable for incompressible two-phase flows with different densities involving only precomputable coefficient matrices. *J. Comput. Phys.* **393**, 229–257.